Geminga's Tails: A Pulsar Bow Shock Probing the Interstellar Medium

P. A. Caraveo,[1]* G. F. Bignami,[2,3] A. DeLuca,[1] S. Mereghetti,[1] A. Pellizzoni,[1] R. Mignani,[4] A. Tur,[2] W. Becker[5]

We report the X-ray Multimirror Mission–Newton European Photon Imaging Camera observation of two elongated parallel x-ray tails trailing the pulsar Geminga. They are aligned with the object's supersonic motion, extend for ~2′, and have a nonthermal spectrum produced by electron-synchrotron emission in the bow shock between the pulsar wind and the surrounding medium. Electron lifetime against synchrotron cooling matches the source transit time over the x-ray features' length. Such an x-ray detection of a pulsar bow shock (with no Hα emission) allows us to gauge the pulsar electron injection energy and the shock magnetic field while constraining the angle of Geminga's motion and the local matter density.

The Geminga pulsar is one of the best-studied isolated neutron stars (*1*). Discovered 30 years ago as a 100-MeV gamma-ray source in Gemini and later identified at x-ray and optical wavelengths, it is known to be at a parallactic distance of ~160 pc (*2*) and to move at 170×10^{-3} arc sec year^{-1} (equivalent to a transverse velocity of 120 km s^{-1}) in the plane of the sky (*3*). Thus, it is one of a few isolated neutron stars with well-defined absolute energetics: Its rotational energy loss, $\dot{E} = 3.2 \times 10^{34}$ erg s^{-1}, is dominated by gamma-ray emission (10^{33} erg s^{-1} in the tens-of-MeV to few-GeV range for a 1 steradian beaming), implying the presence of a relativistic pulsar wind flowing out of the neutron star.

Its soft x-ray emission led to Geminga's identification as a neutron star (*4*) with pulsations at 237 ms (*5*) and with thermal and non-thermal components (*6*) in its x-ray spectrum. The European Photon Imaging Camera (EPIC) onboard XMM-Newton performed a 100-ks exposure on Geminga on 4 April 2002. Whereas the two metal oxide semiconductor (MOS) EPIC cameras were operated with the medium filter in full frame mode (*7*), the positive-negative (pn) camera was operated with the thin filter in small-window mode to allow for the accurate timing of Geminga photons (*8*). The

data were processed with the XMM–Newton Science Analysis Software (SAS) (*9*). After removing time intervals with high particle background and correcting for the dead time, we obtained net exposure times of 55.0 ks for the pn camera and 76.9 and 77.4 ks for MOS1 and MOS2, respectively.

Inspection of both MOS images revealed an extended x-ray feature trailing Geminga (fig. S1 and Fig. 1), with a symmetric structure consisting of two tails ~2 arc min long, or ~0.1 pc at 160 pc. Although such tails originate from or close to Geminga, their morphology within 1′ from the source position cannot be studied because of Geminga's brighter emission. The tails are aligned and symmetric with respect to

the pulsar proper motion vector (Fig. 1). No diffuse emission is detected in the region between the tails, both of which are ~20″ to 30″ thick and therefore only marginally resolved along this dimension, considering the instrument response and the limited statistics. Both tails are highly significant, with a signal-to-noise ratio of 13 in the energy range from 0.3 to 5 keV. The pn data also show the tails; however, owing to the small-window operating mode, the instrument field of view is too small to allow the selection of suitable background regions, thus hampering a detailed analysis of the diffuse emission.

The spectrum of both tails can be described by a power law with an absorption consistent with that observed for the pulsar, $N_{\rm H} = 1.1 \times 10^{20}$ cm^{-2} (*6*), a value for which the photon index of the 450-count tails spectrum is 1.6 ± 0.2 (fig. S2). In the energy range from 0.3 to 5 keV, the total unabsorbed flux from the region is ~2.1×10^{-14} erg cm^{-2} s^{-1}, corresponding to a luminosity of 6.5×10^{28} erg s^{-1}, or ~2×10^{-6} of Geminga's rotational energy loss.

To ascertain possible point source contributions to the extended emissions, we have superimposed our data to the multicolor image library that we have available for Geminga. The faint source 2 arc min northwest of Geminga is associated with an 11-magnitude (mag) K star, whereas in the area covered by our extended emission we note only the presence of a 13-mag late-type star at a position roughly coincident with the end of the southern tail and a 14-mag one about halfway down the tail. Even under the most favorable assumptions of the ratio between the optical and x-ray flux values for

Fig. 1. Inner part of the Geminga EPIC MOS1 and MOS2 images summed together shown after Gaussian smoothing (the raw data can be seen in fig. S1). North is up; east is left. Events in the energy range from 0.3 to 5.0 keV are displayed. Net exposure time is ~77 ks per camera. The Geminga count rates are 0.083 ± 0.001 count s^{-1} and 0.084 ± 0.001 count s^{-1} for MOS1 and MOS2, respectively. Two elongated tails of diffuse emission are seen to emerge from the source, the point spread function of which dominates

the count rate up to an angular distance of ~1′. The tails are ~2′ long and cover an area of ~2 square arc min. The diffuse emission shows a remarkable symmetry with respect to the pulsar proper motion vector, marked by the arrow. The tails' total flux is ~2% of that of Geminga in the energy range from 0.3 to 5 keV.
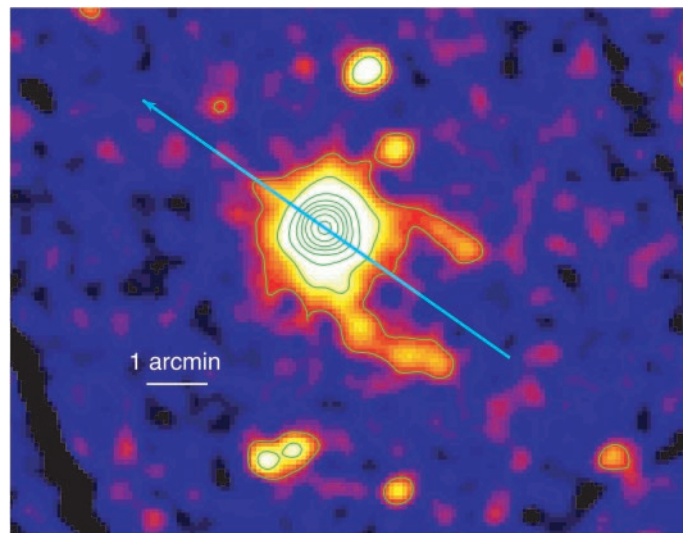
[1]Istituto di Astrofisica Spaziale e Fisica Cosmica–Consiglio Nazionale della Richerche, Via Bassini, 15-20133 Milano, Italy. [2]Centre d'Etude Spatiale des Rayonnements/CNRS–Universite Paul Sabatier, 9 Avenue du Colonel Roche, Toulouse, France. [3]Università di Pavia, Dipartimento di Fisica Teorica e Nucleare, Via Ugo Bassi, 6 Pavia, Italy. [4]European Southern Observatory (ESO), Karl Schwarzschild Strasse 2, 85748 Garching, Germany. [5]Max Planck Institute fur Extraterrestrische Physik, Giessenbachstrasse, 85748 Garching, Germany.

*To whom correspondence should be addressed. E-mail: pat@mi.iasf.cnr.it

late-type stars (*10*), such contaminating sources could yield at most 50 counts out of the 450 ascribed to the sum of the two tails, whose spectral parameters thus remain unchanged when excluding such stars' potential contribution. No other point source contamination to the extended emission is apparent.

The x-ray structure around Geminga is different from those seen around other pulsars (*11–13*). Its shape, characterized by two parallel streams with no detectable emission in between, gives the impression of the projected view, in the plane of the sky, of an empty paraboloid or cone of x-ray emission. Because similar velocity-driven, arc-shaped features have been seen in Hα around a few pulsars (*14, 15*), we have obtained a deep Hα plate of the region. The data were collected at the ESO Very Large Telescope (VLT)–ANTU telescope in February 2003 for a total exposure of 5 hours with the use of the Focal Reducer/Low Dispersion Spectrograph 1 (FORS1) instrument. In the confused interstellar medium (ISM) at these low galactic latitudes ($b = +4.2$), no organized diffuse Hα emission is observed from the x-ray structure surrounding Geminga. The resulting image (Fig. 2) together with the x-ray isophotes allows us to calculate an upper limit to the Hα emission of 10^{-18} erg cm^{-2} arc sec^{-2}.

The fraction of the spin-down energy channeled by Geminga into its x-ray tails is two orders of magnitude lower than the values measured for the nebulae of PSR1757-24 (*11*), PSR1929+10 (*12*), and PSR B1957+20 (*13*). To date, few (if any) pulsars can rely on observing times long enough to allow for the detection of comparably faint features. In this case, the proximity of Geminga has played a crucial role so that we are here confronted with yet another first in the phenomenology of Geminga.

The geometry of the extended emission may be modeled as a bow shock formed at the equilibrium region between the pulsar energy loss, $\dot{E}$, and the dynamical pressure generated by its supersonic motion in the ISM. Ram pressure balance between a spherical relativistic pulsar wind and the ambient medium determines the stand-off radius, R_{SO}, of the bow shock, i.e., the distance from the pulsar to the shock front:

$$\frac{\dot{E}}{4\pi R_{SO}^2 c} = \rho_{ISM} V_{NS}^2 \qquad (1)$$

where ρ_{ISM} is the density of the interstellar medium, V_{NS} is the pulsar velocity $V_{NS} = \mu D/\cos i$ (μ is proper motion, D is distance, and i is inclination angle to the plane of sky, for which $i = 0$), and $\dot{E}$ is the rotational energy loss going into the relativistic wind. For simplicity, we have assumed such a wind to be spherically symmetric at the distance R_{SO}. Collimated energy outflow in the form of beams and jets complicates only slightly the geometry but not the energetics of the problem.
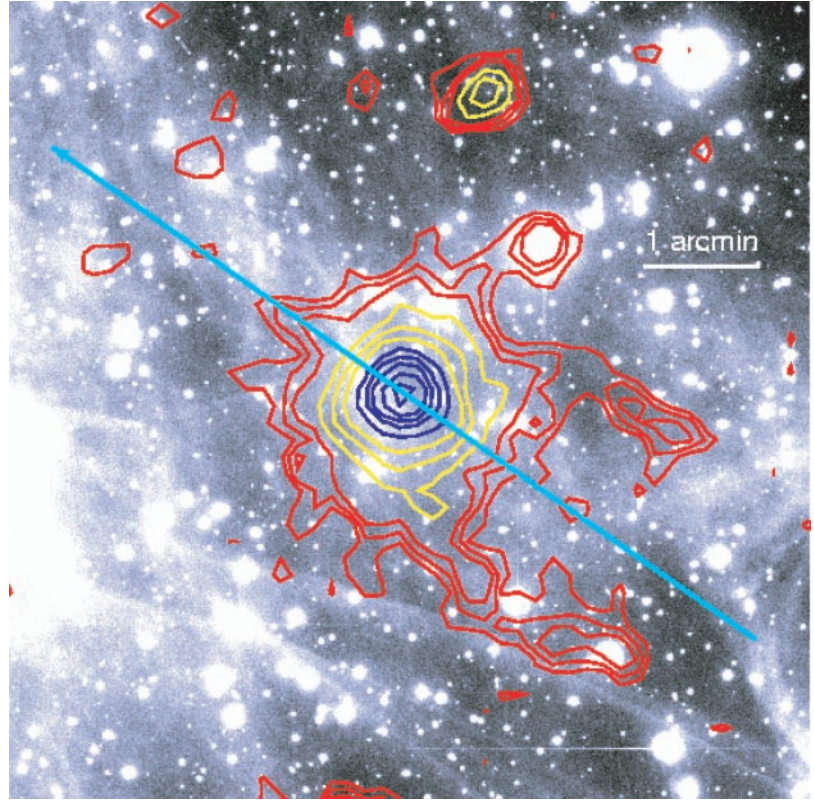
Fig. 2. Deep (5 hours) VLT FORS1 image of the Geminga field in the Hα band ($\lambda = 6563$ A, $\Delta\lambda = 61$ A). North is up; east is left. The isophotes of the x-ray image are overlaid (three different steps in surface brightness level have been used: 20%, red; 50%, yellow; and 100%, blue). No Hα emission correlated with the x-ray tails can be seen. It is also evident that no bright sources are present in the region covered by the tails, with the exception of the southwest edge, where a 13-mag late-type star is seen. Its contribution to the x-ray emission, however, is estimated to be marginal.

The distance, proper motion, and spin-down energy of Geminga are known. Thus, its R_{SO} is a function of only two unknown values (the ambient medium density and i), with a negligible error dispersion on the other parameters. We calculated the expected Geminga stand-off angle ($\delta = R_{SO}\cos i/D$) as a function of the inclination angle to the plane of sky and the ISM density (fig. S3). The stand-off angle is not resolved by EPIC, because the brightness ratio between Geminga and its extended feature is so high that the current $<5\%$ uncertainty in the knowledge of the instrument's response to a point source leaves residuals outshining the faint diffuse emission up to 40″ from the central source. Mapping the feature close to Geminga is thus impossible: We can only set a robust upper limit of $\delta < 40″$.

Generalizing momentum balance along directions other than that of the proper motion and assuming a spherical pulsar wind in a homogeneous ISM, we can describe the analytic solution for the axisymmetric three-dimensional shape (*16*) of the bow shock as follows:

$$R_\theta = \frac{R_{SO}\sqrt{3\left(1 - \frac{\vartheta}{\tan\vartheta}\right)}}{\sin\vartheta} \qquad (2)$$

where R_θ is the shock front distance as a function of the angle ϑ from the pulsar direction of motion (Fig. 3, inset).

We compare our data to a three-dimensional geometrical model of the Geminga bow shock based on Eq. 2, obtaining an estimate of R_{SO} independent from all physical parameters described in Eq. 1. The symmetric, two-streamed feature shown in Fig. 1 is reproduced by the projection effect in the plane of the sky of such an emitting surface, assumed uniform, the edges of which show up brighter because of a limb effect.

Applying our geometrical model for different values of i, we see that only bow shocks with inclination angles to the plane of sky $i < 30°$ satisfactorily describe our data (Fig. 3). Thus, Geminga travels at a relatively small angle with respect to the plane of the sky, and $i < 30°$ implies stand-off angle values of $\delta \sim 20″$ to 30″, corresponding to $R_{SO} \sim 6 \times 10^{16}$ cm. This set of values constrains the range for the total ambient medium density to be $0.06 < \rho_{ISM} < 0.15$ atoms cm^{-3}. Such a range agrees with the expected value of the ISM density for the region around Geminga (*17*) and constrains Geminga's Mach number (*M*) to be $14 < M < 20$. More quantitative parameter fitting will have to wait for higher resolution x-ray data.
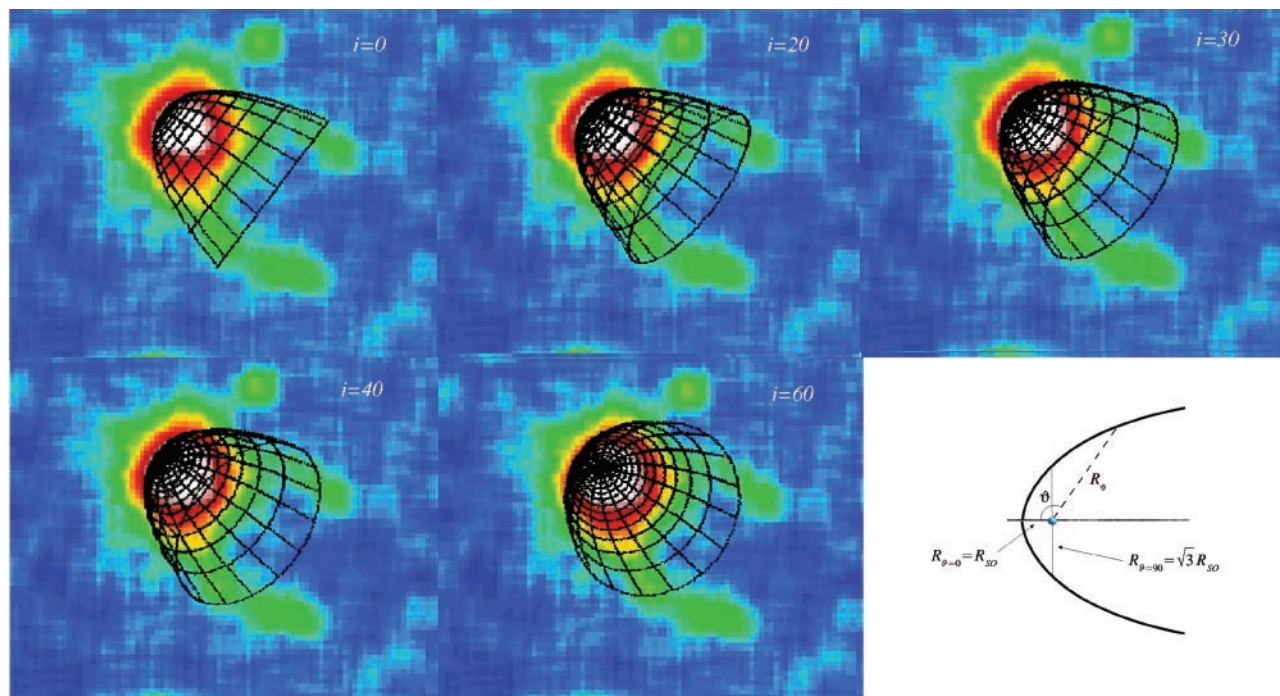
Fig. 3. Comparison of our x-ray data with the three-dimensional bow-shock geometrical models. The cases for inclination angles 0°, 20°, 30°, 40°, and 60° are shown. As apparent, inclination angles $i > 30°$ do not fit the data. For $i < 30°$, the fit constrains the stand-off angle in the range of 20 to 30″. (**Inset**) Bow-shock profile drawn from Eq. 2 as a function of the angle from the proper motion direction (ϑ) and shock front distance (R).

The overall Hα luminosity expected from a bow shock is (18, 19) $L_{Ha} \sim \dot{E} \cdot V_{NS} \cdot X$, where X is the neutral H fraction. Given our Hα upper limit, we deduce a neutral hydrogen fraction <0.01. It is plausible that such a condition could be met in the troubled ISM around Geminga, considering also the presence of the highly ionizing γ- and x-ray pulsar.

As to the physics of the tails, their hard, power-law x-ray spectrum suggests synchrotron emission of energetic electrons in a magnetic field. Although energetic electrons are naturally and copiously supplied by the Geminga γ-ray pulsar, its magnetic field will have decayed to practically zero at the sub-light-year distances of interest here. An appropriate magnetic field is provided by the interstellar one compressed in the bow shock. Because the large-scale interstellar magnetic field can be assumed to be frozen to the ISM, we take advantage of bow-shock theory (20, 21) that, for $M \gg 1$ and $\gamma = 5/3$, yields $\rho_{shock} = 4\rho_{ISM}$, implying a magnetic field $B_{shock} = 4B_{ISM}$, or $\sim 10^{-5}$ G for a typical average ISM magnetic field (22). After the standard magneto-bremmsthrahlung treatment (23), we can estimate that the keV photons of the Geminga tails are produced by electrons up to 10^{14} eV, a value close to the upper energy limit for pulsar wind electrons in Geminga (24). In cooling by synchrotron photon emission, such electrons will Larmor-gyrate in the compressed bow-shock field, with a radius of about 3.4×10^{16} cm. Each tail thickness is then predicted to be

$\sim 6.8 \times 10^{16}$ cm, or $\sim 27″$ at the distance of Geminga, in excellent agreement with our observations (Fig. 1).

A final consideration of the emission physics and geometry supplies an independent consistency check to our model. If synchrotron emission is the major cooling process of the energetic tail electrons, to wit their hard x-ray spectrum, one can compute the lifetime of such electrons (or, more precisely, the time it takes for them to lose half of their energy) in the bow-shock magnetic field. This turns out to be ~ 800 years. On the other hand, Geminga's proper motion (170×10^{-3} arc sec year^{-1}) allows one to compute the time taken by the pulsar and its bow shock to transit over the apparent length of the x-ray structures in the sky ($\sim 3′$ from the central source). Such a time is close to 1000 years. Thus, Geminga's tails remain visible for a time comparable to the electron synchrotron x-ray emission lifetime after the pulsar passage.

The diffuse emission reported here, although containing only 10^{-6} of the pulsar rotational energy loss, provides a direct gauge both of the pulsar wind electron energy (10^{14} eV) and of the local interstellar magnetic field (2 to 3 μG) under the simple assumptions of the synchrotron nature of the tails emission.

References and Notes
1. G. F. Bignami, P. A. Caraveo, *Annu. Rev. Astron. Astrophys.* **34**, 331 (1996).
2. P. A. Caraveo *et al.*, *Astrophys. J.* **461**, L1 (1996).
3. G. F. Bignami, P. A. Caraveo, S. Mereghetti, *Nature* **361**, 704 (1993).
4. G. F. Bignami, P. A. Caraveo, R. C. Lamb, *Astrophys. J.* **272**, L9 (1983).
5. J. P. Halpern, S. S. Holt, *Nature* **357**, 222 (1992).
6. J. P. Halpern, F. Y.-H. Wang, *Astrophys. J.* **477**, 905 (1997).
7. M. Turner *et al.*, *Astron. Astrophys.* **365**, L27 (2001).
8. L. Strüder *et al.*, *Astron. Astrophys.* **365**, L18 (2001).
9. SAS, 5.3.3, available at http://xmm.vilspa.esa.es/external/xmm_sw_cal/sas_frame.shtml.
10. J. Krautter *et al.*, *Astron. Astrophys.* **350**, 743 (1999).
11. V. M. Kaspi *et al.*, *Astrophys. J.* **562**, L163 (2001).
12. Q. D. Wang *et al.*, *Nature* **364**,127 (1993).
13. B. W. Stappers *et al.*, *Science* **299**,1372 (2003).
14. S. Chatterjee, J. M. Cordes, *Astrophys. J.* **575**, 407 (2002).
15. B. M. Gaensler *et al.*, *Astrophys. J.* **580**, L137 (2002).
16. F. P. Wilkin, *Astrophys. J.* **459**, L31 (1996).
17. N. Gehrels, W. Chen, *Nature* **361**, 706 (1993).
18. J. M. Cordes *et al.*, *Nature* **362**, 133 (1993).
19. A. Pellizzoni, A. De Luca, S. Mereghetti, *Astron. Astrophys.* **393**, L65 (2002).
20. S. N. Shore, *An Introduction to Astrophysical Hydrodynamics* (Academic Press, New York, 1992), p. 107.
21. C. F. McKee, D. J. Hollenbach, *Annu. Rev. Astron. Astrophys.* **18**, 219 (1980).
22. K. R. Lang, *Astrophysical Formulae* (Springer Verlag, Berlin, 1992), p. 52.
23. V. L. Ginzburg, S. I. Syrovatskii, *Annu. Rev. Astron. Astrophys.* **3**, 297 (1965).
24. J. Halpern, M. Ruderman, *Astrophys. J.* **415**, 286 (1993).
25. It is a pleasure to thank the ESO Director General for granting Director Discretionary time for our Hα observation, which was rapidly carried out in service mode by the Paranal staff. The XMM-Newton data analysis is supported by the Italian Space Agency (ASI). A.D.L. acknowledges an ASI fellowship.